Q. J. R. Meteorol. Soc. (2001), **127**, pp. 1–17

The dependence of thunderstorm evolution on the initial convective trigger

By LEWIS GRASSO *

(Received 1 June 2001; revised 1 June 2001)

SUMMARY

Previous studies have emphasized the use of a minimum bubble to trigger thunderstorms in an idealized simulation. Reducing the influence of the bubble on long-term solutions was the reason. A mesoscale model was used to simulate the dependence of thunderstorm behavior on bubble characteristics. Although past work favors the minimum bubble, a vigorous bubble was required for the simulated thunderstorm to behave like the observed thunderstorm.

KEYWORDS: Warm Bubble Initialization

1. INTRODUCTION

Numerically simulated thunderstorms have been triggered by either a warm or cold bubble. The dimensions of a typical bubble used in previous studies were approximately 20 km in the horizontal direction and 2 km vertically. Because values of temperature and water vapor mixing ratio within the bubble were different from the environment, thunderstorms developed. One warm bubble has been sufficient to trigger a supercell thunderstorm; several warm bubbles have been used to initiate a squall line. In some cases, simulated squall lines were triggered with a cold bubble. Further details about the characteristics of some bubbles may be found in the following articles: Weisman and Klemp (1982), Dudhia and Moncrieff (1989), and Grasso (2000).

Some researchers have emphasized the use of a mininum bubble to trigger simulated thunderstorms. Consider the following examples: "The magnitude of this perturbation represents the minimum value necessary to produce consistent development of an initial convective cell within the experimental range of envinronmental conditions." (Weisman and Klemp, 1982), "These thermal amplitudes are approximately the smallest that could be used to create convection that persists into the second hour in all simulations within the two CAPE regimes, given the prescribed shears." (McCaul and Weisman, 2001), "The scale of the cooling region appears to be near the minimum necessary to generate a self-sustaining system under these environmental conditions because a 10 km radius impulse failed." (Dudhia and Moncrieff, 1989), and "This thermal perturbation was near the minumum magnitude that would produce storm initiation within a reasonable time (i.e., 20-30 min) for all cases considered." (Bluestein and Weisman, 2000). Justification for the use of a minimun bubble can be found in Bluestein and Weisman (2000); they state, "Using the minumum perturbation is important to ensure that the long-term solutions are minimally affected by the nature of the initialization."

A solution to a system of differential equations is uniquely determined by an initial state. In other words, once an initial state has been prescribed the long-term solution will be predetermined: Before a numerical model is advanced one time step. Therefore, choosing an initial state to ensure that long-term solutions are minimally affected by the nature of the initialization is impossible: Long-term solutions are uniquely determined by the initial state. Emphasis on the use of a minimum bubble–to simulate a thunderstorm–might be misleading: suggesting that thunderstorm development in the Earths atmosphere only results from minimal forcing. Vigorous triggering might lead to unexpected characteristics of a thunderstorm, for thunderstorm behavior may depend not only on the environment but also on the force of initiation.

* Corresponding author: Cooperative Institute for Research in the Atmosphere Fort Collins, Colorado 80523, USA. e-mail: grasso@cira.colostate.edu

Several papers in the literature have emphasized the use of a minimum bubble to trigger a simulated thunderstorm. The dearth of studies on convective triggering provided the motivation to examine the relationship between thunderstorm characteristics and the vigor of convective initiation. This study relates to previous work by examining the emphasis to use a minimum bubble to trigger a simulated thunderstorm. The original aspect of this work is the examination of the relationship between thunderstorm morphology and the vigor of convective initiation.

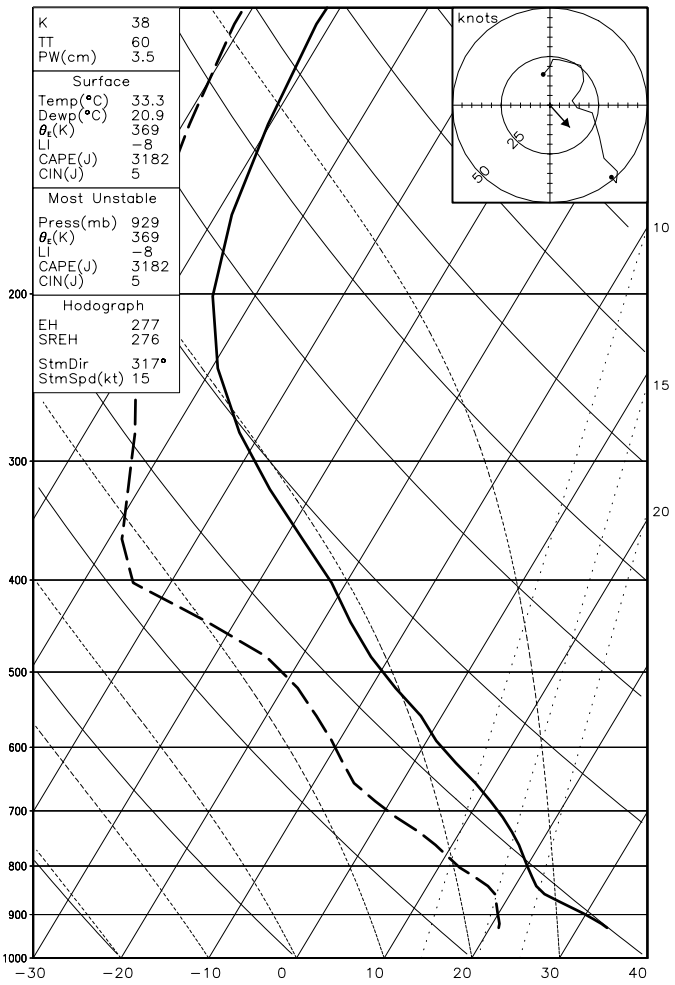

Figure 1. Sounding used to initialize the domain. The left vertical axis is pressure (mb); the right vertical axis is water vapor mixing ratio (g kg^{-1}), and the horizontal axis is temperature (°C).

2. Computational Methodology

The numerical model used for this simulation was the Regional Atmospheric Modeling System (RAMS) developed at Colorado State University (Pielke et al. 1992). The following features were used to run the model:

- Non-hydrostatic and compressible (Tripoli and Cotton 1982).

• Momentum was advanced using a leapfrog scheme; scalars were advanced using a forward scheme: Both methods used second order advection.

• Vertical and horizontal turbulence were parameterized using a Smagorinsky deformation based eddy viscosity (Smagorinsky 1963) with stability modifications (Lilly 1962).

• Hydrometers were predicted with a new two-moment bulk microphysical scheme (Meyers et al. 1997). Mixing ratio and concentration were prognosed; mean diameter was diagnosed. The following hydrometeor species were included in the simulations: cloud droplets, rain droplets, aggregates, grauple, hail, snow, and pristine ice.

• Other prognostic variables were the three components of momentum–u, v, w; Exner function, π; total water, r_t; and ice-liquid potential temperature, θ_{il} (Tripoli and Cotton 1981).

• Arakawa fully staggered C grid (Arakawa and Lamb 1981).

• Exner function tendencies used to update the momentum variables were computed using a time split scheme, similar to Klemp and Wilhelmson (1978).

• Lateral boundaries used the Klemp-Wilhelmson condition, in which the normal velocity component specified at the lateral boundary is effectively advected from the interior.

• A wall was specified at the top boundary with friction layers below.

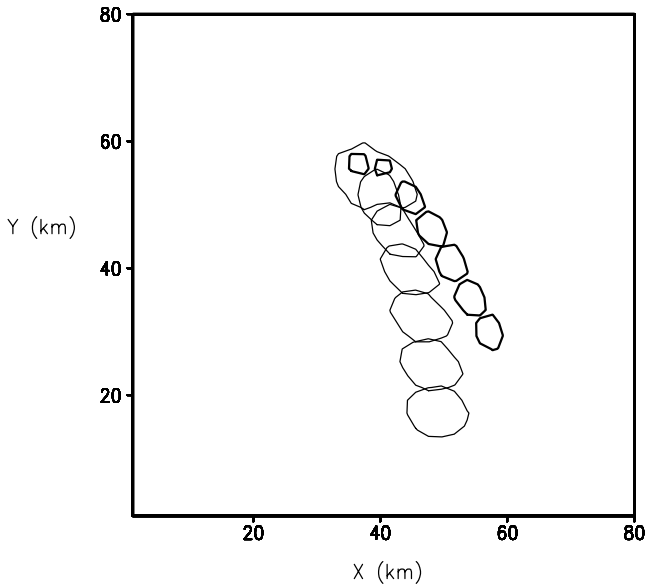

Figure 2. Position of the 15 m s^{-1} updraft contour–every fifteen minutes–near 5 km. The updraft in R1 is represented by a thin contour; the updraft in R2 is represented by a thick contour.

Configuration of the grid was similar methods used in previous work. Horizontal grid spacings of 2 km were used within a domain spanning 80 km x 80 km. The domain extended to a height of approximately 23 km. The vertical grid spacing started at 100 m and was stretched by a factor of 1.1 until the value reached 2000 m; from that height to the top of the domain the vertical grid spacing had a constant value of 2000 m. A time step of 5 s was used in several simulations, each spanning two hours.

Initialization of the domain was similar to that of Grasso (2000). The sounding used to initialize the horizontally homogeneous environment (Fig. 1) was retrieved from the Geostationary Operational Environmental Satellite (GOES) 11 at 2146 UTC 24 July 2000 near 41 N and 99.5 W: south central Nebraska. Vertical wind profiles from Neligh and McCook, Nebraska were used to initialize the winds within the domain.

In several simulations, convection was triggered by an instantaneous warm bubble. In the first simulation, referred to as R1, the interior of the bubble had a spacially constant temperature excess of 3 ^{0}K and a spacially constant water vapor excess of twenty percent. In the final simulation, referred to as R2, the interior of the bubble had the same temperature excess as R1; however, the spacially constant water vapor excess was decreased to five percent. For the other simulations, the temperature excess–within each bubble–was identical to the temperature excess within the bubble used in R1; however, the water vapor excess ranged between five and twenty percent. Each bubble was 11 x 11 points in the horizontal and extended upward from 50 m to approximately 2600 m. During all simulations, radiational processes were excluded; values of sensible and latent heat fluxes were set to zero.

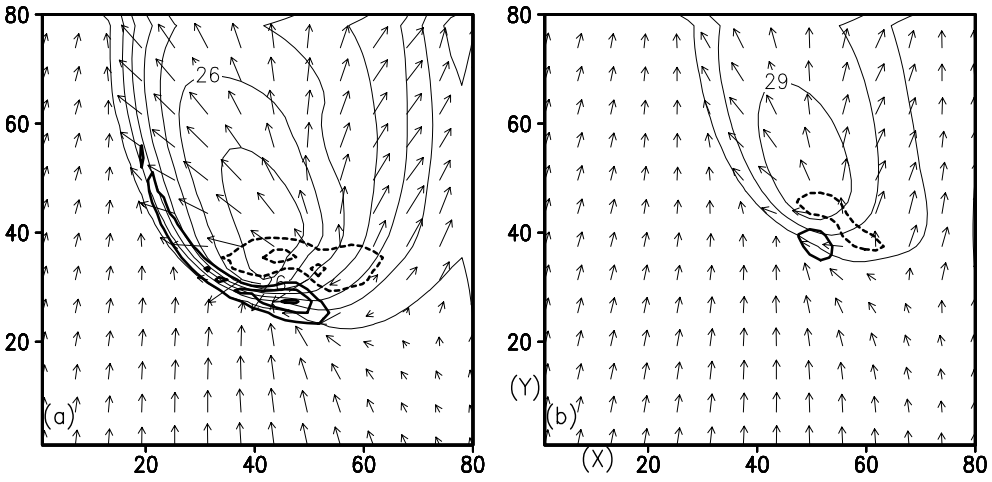

Figure 3. Horizontal wind vectors, vertical motion–thick contours, and temperature–thin contours, near 50 m at 1 hour and 35 minutes into (a) R1 and (b) R2. Contoured values of vertical motion were -0.6, -0.3, 0.3, 0.6, and 0.9 m s^{-1}; temperature was contoured every 1 ^{o}C.

3. Comparison of R1 and R2

Because of the emphasis placed on using a minimum bubble to trigger convection, several simulations were conducted. To begin with, the bubble used in R1 was duplicated from a past simulation. Values of water vapor mixing ratio interior to the bubble were reduced in successive simulations until convective triggering failed. As a result, the bubble used in R2 provided the minimum forcing that allowed thunderstorm development.

Results from R1 and R2 exhibited some differences. For example, the updraft at midlevels in R1 moved faster–8 m s^{-1} compared to 7 m s^{-1}, more to the right–350^o compared to 330^o, and had a larger horizontal length scale–7 km compared to 5 km–relative to the updraft in R2 (Fig. 2). Near the surface, cold pool temperatures were lower in R1 than in R2; in addition, the cold pool in R1 expanded over a greater area

than the cold pool in R2 (Fig. 3). Not only did the vertical motions of the thunderstorm have a greater amplitude, but also the storm produced outflow wind speeds that were larger in R1 than in R2. The simulated thunderstorm in R1 also produced more surface condensate over a larger area than the thunderstorm in R2 (Fig. 4). The leading edge of the cold pool, near the thunderstorm at x=40 and y=30, was oriented approximately east-west in R1 (Fig. 4a); in contrast, the leading edge of the cold pool in R2, near x=50 and y=40, was oriented approximately northwest-southeast (Fig. 4b). If considering only the environment of the thunderstorm–that is, the sounding and hodograph, nowcasting the behavior of storms–such as those in R1 and R2–could be a difficult task.

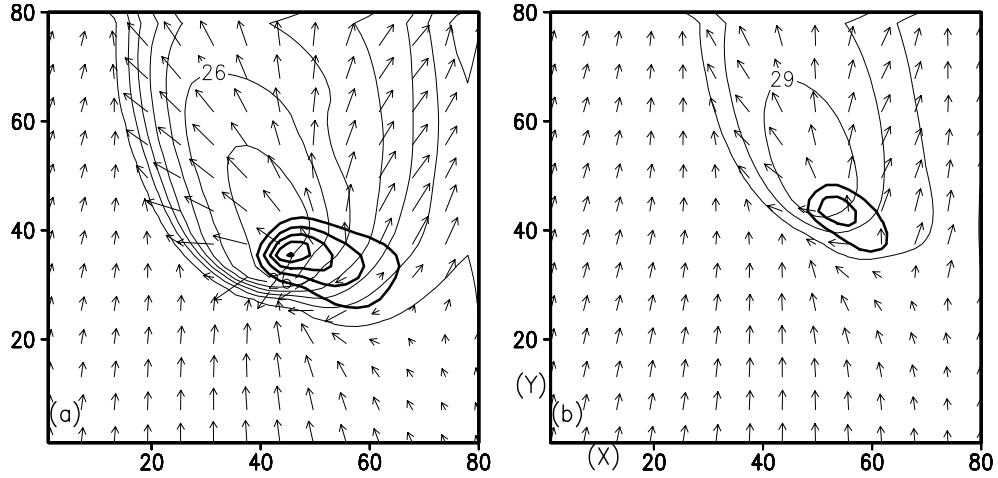

Figure 4. Same as Fig. 3 except the thick contours represent total condensate mixing ratio. Values of condensate that were contoured are 0.5, 1.0, 1.5, 2.0, and 2.5 g kg^{-1}.

4. Simulated Tendencies of Vertical Motion

Although the environment was the same in R1 and R2, the thunderstorm in R1 was more vigorous than the thunderstorm in R2. Insight about the different characteristics exhibited by the two thunderstorms was provided by analyzing all tendency terms in the vertical equation of motion. The vertical equation of motion used by RAMS is written as

$$\frac{\partial w}{\partial t} = -\frac{1}{\rho_o}\{\frac{\partial}{\partial x}(\rho_o uw) + \frac{\partial}{\partial y}(\rho_o vw) + \frac{\partial}{\partial z}(\rho_o ww)\}$$

$$-\theta_o \frac{\partial \pi^*}{\partial z} + (\frac{\theta_v - \theta_o}{\theta_o} - r_c)g$$

$$+\frac{1}{\rho_o}\{\frac{\partial}{\partial x}(\rho_o k_h \frac{\partial w}{\partial x}) + \frac{\partial}{\partial y}(\rho_o k_h \frac{\partial w}{\partial y}) + \frac{\partial}{\partial z}(\rho_o k_v \frac{\partial w}{\partial z})\}. \quad (1)$$

There are four tendency terms on the right hand side of Eq. 1: advection, $-\frac{1}{\rho_o}\{\frac{\partial}{\partial x}(\rho_o uw) + \frac{\partial}{\partial y}(\rho_o vw) + \frac{\partial}{\partial z}(\rho_o ww)\}$; vertical π^* gradient, $-\theta_o \frac{\partial \pi^*}{\partial z}$; buoyancy, $(\frac{\theta_v - \theta_o}{\theta_o} - r_c)g$; and turbulent mixing, $\frac{1}{\rho_o}\{\frac{\partial}{\partial x}(\rho_o k_h \frac{\partial w}{\partial x}) + \frac{\partial}{\partial y}(\rho_o k_h \frac{\partial w}{\partial y}) + \frac{\partial}{\partial z}(\rho_o k_v \frac{\partial w}{\partial z})\}$. The following variables

are contained in Equation 1: All three components of the wind vector–u, v, w; base state potential temperature, θ_o; base state density, ρ_o; virtual potential temperature, θ_v; total water condensate mixing ratio, r_c; acceleration of gravity, g; perturbation Exner function, π^*; parameterized horizontal mixing coefficient, k_h; and the parameterized vertical mixing coefficient, k_v.

Values of all four terms on the right hand side of Eq. 1 were saved, combined to generate $\frac{\partial w}{\partial t}$, and contoured in Fig. 5. Although Fig. 5 was made from model output at the same time as Figs. 3 and 4, a smaller portion of the domain was chosen for display. As alluded to earlier, both the cross sectional area and the maximum updraft speed were larger in the thunderstorm in R1 (Figs. 5a, 5c, 5e) compared to the thunderstorm in R2 (Figs. 5b, 5d, 5f). In addition, the pattern of values of $\frac{\partial w}{\partial t}$ was similar between R1 and R2; that is, the approximate east-west region where $\frac{\partial w}{\partial t}$ was negative was bounded to the north and south by regions where $\frac{\partial w}{\partial t}$ was positive (Figs. 5a-5d). The northern most region where $\frac{\partial w}{\partial t}$ was positive acted to increase the downdraft speed–the downdraft was omitted from Fig. 5 for readability. At higher levels (Figs. 5e and 5f) the pattern of $\frac{\partial w}{\partial t}$ was similar between R1 and R2; specifically, the region where $\frac{\partial w}{\partial t}$ was negative was northward of the region where $\frac{\partial w}{\partial t}$ had positive values. Similar to the comparison between the updrafts, both the area where $\frac{\partial w}{\partial t}$ differed from zero and the amplitude of values of $\frac{\partial w}{\partial t}$ were larger in and around the thunderstorm in R1 than the thunderstorm in R2: Compare Figs. 5a with 5b, 5c with 5d, and 5e with 5f. Near the surface, positive values of $\frac{\partial w}{\partial t}$ along the forward edge of the main and flanking updraft in R1 (Fig. 5a) were larger than all positive values of $\frac{\partial w}{\partial t}$ associated with the updraft in R2 (Fig. 5b). Lastly, the orientation of $\frac{\partial w}{\partial t} = 0$ that bisected the updraft in R1 was approximately east-west (Figs. 5a, 5c, 5e); however, the same value bisected the updraft in R2 in a southwest-northeast direction (Figs. 5b, 5d, 5f).

5. Physical Interpretation

Physical interpretation of Figs. 2-5 provides an explanation of the differences between the thunderstorm in R1 and the thunderstorm in R2. For example, the thunderstorm in R1 was always more vigorous than the thunderstorm in R2. That is, not only were the area and speed of the updraft larger in the thunderstorm in R1, compared to the thunderstorm in R2, but also the area and amplitude of upward acceleration were larger within the forward flank of the storm in R1 (compare Figs. 5a with 5b and 5c with 5d). Even though the convective available potential energy was the same in R1 and R2, greater upward motion near the level of free convection led to greater upward motion at midlevels of the thunderstorm in R1 (Fig. 5e) compared to the storm in R2 (Fig. 5f). Because both the cross sectional area and speed of the updraft were larger in R1, the storm ingested a greater mass of water vapor compared to the storm in R2. As a result, the thunderstorm in R1 produced more condensate near the surface (Fig. 4). Evaporation of more condensate produced more cooling, a faster downdraft, and a cooler cold pool (compare Figs. 3a with 3b). This sequence caused the storm in R1 to have the following characteristics: Faster outflow winds–which caused the cold pool to expand over a relatively large area (Fig. 4), more convergence and upward acceleration along the outflow boundary, and larger upward motion over a greater area below the level of free convection (Figs. 5a and 5b). Although the above process was self-sustaining, a lifting mechanism was required initially: The mechanism was the warm bubble used in R1.

Although the environment of each thunderstorm was the same (Fig. 1), the speed and direction of the thunderstorms differed (Fig. 2). Values of $\frac{\partial w}{\partial t}$ had a larger magnitude

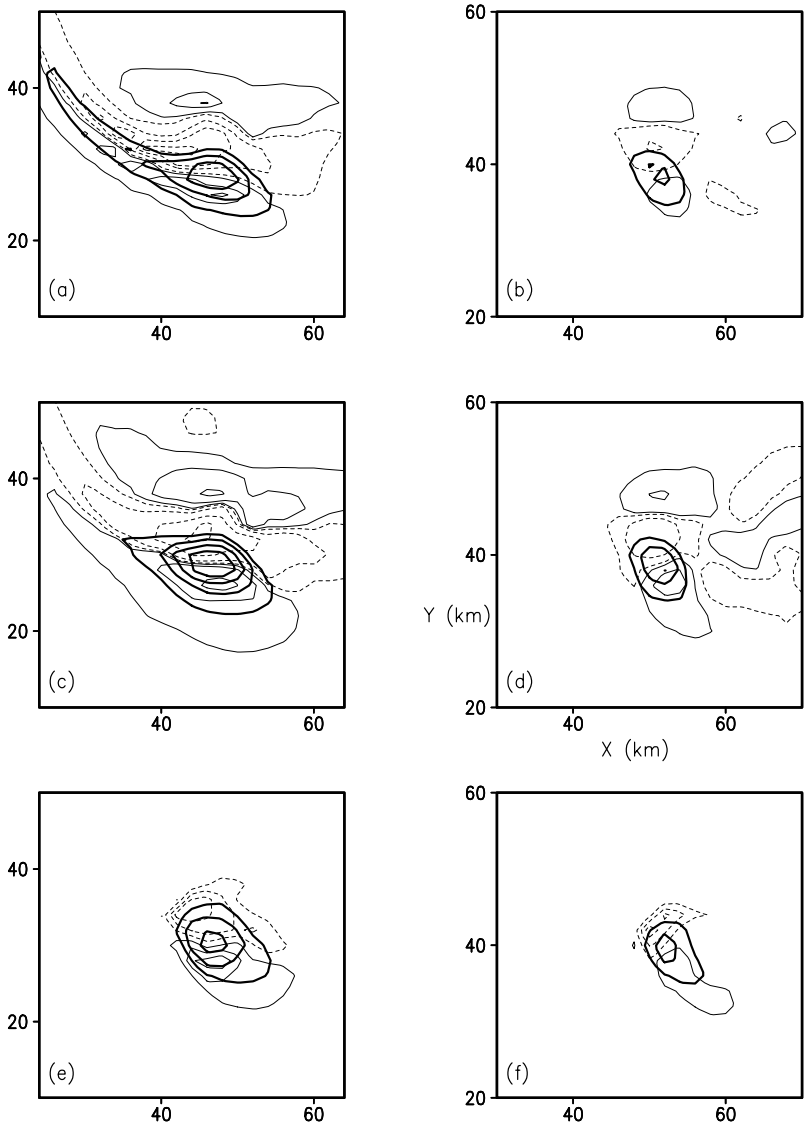

Figure 5. Upward motion–thick contours–and $\frac{\partial w}{\partial t}$–thin contours–at one hour and thirty five minutes into R1 and R2. Results from R1 are displayed in (a), (c), (e) while (b), (d), (f) show results from R2. Three levels are shown: 400 m–(a), (b); 1.2 km–(c), (d); and 5 km–(e), (f). Values of $\frac{\partial w}{\partial t}$ contoured in (a) and (b) are -11, -8, -5, -1, 1, 5, and 8 x 10^{-3} m s^{-2}; in (c) and (d) the values are -25, -15, -5, -1, 1, 5, and 15 x 10^{-3} m s^{-2}; lastly, -50, -30, -10, 10, 30, and 50 x 10^{-3} m s^{-2} in (e) and (f). Values of upward motion contoured in (a) and (b) are 1, 2, and 3 m s^{-1}; in (c) and (d) the values are 2, 4, 6, and 8 m s^{-1}; lastly, 10, 20, and 30 m s^{-1} in (e) and (f).

about the updraft in R1 than they exhibited about the updraft in R2 (Fig. 5). Therefore, the updraft in R1 moved a larger horizontal distance for a given unit of time. Relatively large lifting occurred along the gust front that extended westward from the thunderstorm in R1 (Fig. 5a); in addition, upward lifting existed to the west of the updraft core near 1.2 km (Fig. 5c). Lifting along the outflow boundary caused the development of upward

motion to the west of the updraft core in R1: Note the westward extension of the updraft in R1 (Fig. 5c). Lifting along the gust front was absent to the west of the updraft in R2; in fact, $\frac{\partial w}{\partial t}$ had negative values to the west of the updraft (Fig. 5d). Even though the environmental winds were identical in both simulations, enhanced lifting along the gust front caused the thunderstorm in R1 to move to the right of the thunderstorm in R2.

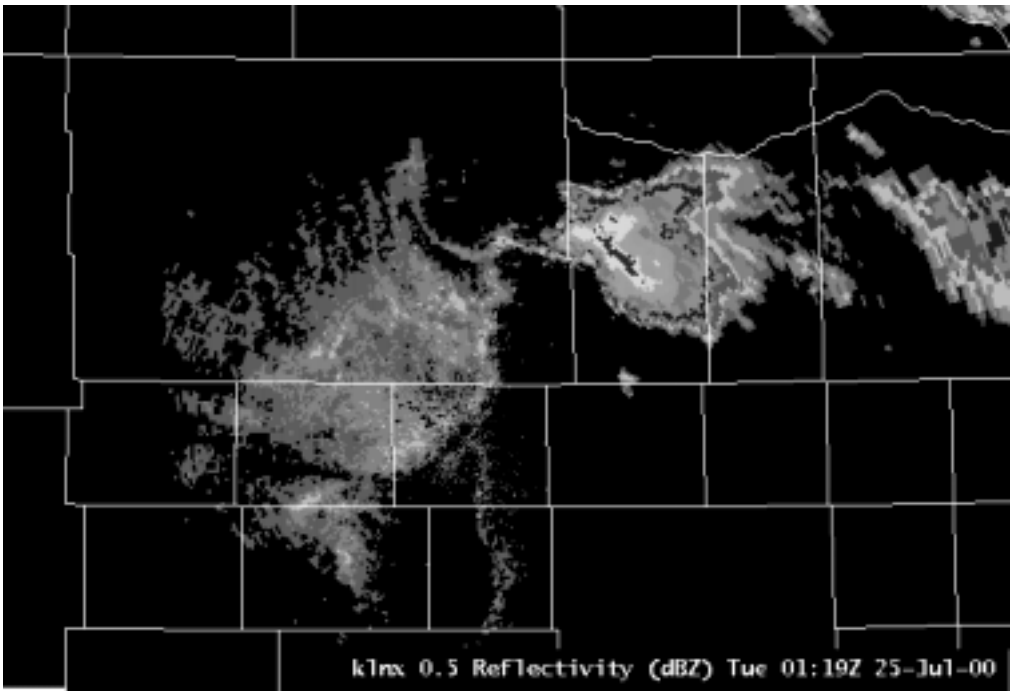

Figure 6. Reflectivity at 0.5^o from the North Platte, Nebraska Doppler radar (KLNX) on 25 July 00 at 0119 UTC.

Which simulation is preferred? Based on past research, the simulation that used the minimum bubble, R2, would be favored; observations, however, support some of the results of R1. Storm motion, which was derived from the North Platte, Nebraska, Doppler radar (KLNX), was from 350^o at 12 m s^{-1}. When the thunderstorm was relatively close to the radar, the outflow boundary extended westward from the precipitation field (Fig. 6). Support for simulated updraft growth above the gust front in R1 was provided by visible satellite imagery; that is, new cumulus towers were observed developing to the west of the parent updraft. Although some differences did occur between the observed and simulated thunderstorm in R1, storm motion in R1 was more similar to the observed storm than the motion of the thunderstorm in R2.

6. Conclusions

The dependence of thunderstorm morphology on the initial convective trigger was explored by using a numerical model. Results indicate that the vigor of the convective trigger may be as important as the environment in determining storm behavior. In R1, greater initial lifting caused larger upward motion below the level of free convection, increased mass flux of water vapor into the thunderstorm, more condensate that fell into the boundary layer, a cooler cold pool that expanded over a greater area, faster outflow

winds, more convergence in the subcloud layer, and greater upward motion below the level of free convection. That is, the more forceful initial trigger used in R1 led to a self-sustaining process that caused the thunderstorm to be more vigorous, move faster, and to the right of the storm in R2. Compared to the storm triggered by the minimum bubble, the storm in R1 exhibited motion that was more similar to the observed thunderstorm.

Acknowledgements

This material is based on work supported by the National Oceanic and Atmospheric Administration under Grant No. NA67RJ0152. Thanks are extended to Dr. Mark DeMaria for his helpful comments.

References

Arakawa, A., and Lamb, V. 1981 A potential enstrophy and energy conserving scheme for the shallow water equations. *Mon. Wea. Rev.*, **109**, 18–36

Bluestein, H. B., and Weisman, M. L. 2000 The interaction of numerically simulated supercells initiated along lines. *Mon. Wea. Rev.*, **128**, 3128–3149

Dudhia, J., and Moncrieff, M. W. 1989 A three-dimensional numerical study of an Oklahoma squall line containing right-flank supercells. *J. Atmos. Sci.*, **46**, 3363–3391

Grasso, L. D. 2000 The dissipation of a left moving cell in a severe storm environment. *Mon. Wea. Rev.*, **128**, 2797–2815

Klemp, J. B., and Wilhelmson, R. B. 1978 The simulation of three-dimensional convective storm dynamics. *J. Atmos. Sci.*, **35**, 1070–1096

Lilly, D. K. 1962 On the numerical simulation of buoyant convection. *Tellus*, **14**, 148–172

McCaul, E. W., and Weisman, M. L. 2001 The sensitivity of simulated supercell structure and intensity to variations in the shapes of environmental buoyancy and shear profiles. *Mon. Wea. Rev.*, **129**, 664–687

Meyers, M. P., Walko, R. L., Harrington, J. Y., and Cotton, W. R. 1997 New RAMS cloud microphysics parameterization. Part II: The two-moment scheme. *Atmos. Res.*, **45**, 3–39

Pielke, R. A., Cotton, W. R., Walko, R. L., Tremback, C. J., Lyons, W. A., Grasso, L. D., Nicholls, M. E., Moran, M. D., Wesley, D. A., Lee, T. J., and Copeland, J. H. 1992 A comprehensive meteorological modeling system-RAMS. *Meteor. and Atmos. Phys.*, **49**, 69–91

Smagorinsky, J. 1963 General circulation experiments with the primitive equations. Part 1: The basic experiment. *Mon. Wea. Rev.*, **91**, 99–164

Tripoli, G. J., and Cotton, W. R. 1982 The Colorado State University three dimensional cloud mesoscale model. Part I: General theoretical framework and sensitivity experiments. *J. Rech. Atmos.*, **16**, 185–220

Tripoli, G. J., and Cotton, W. R. 1981 The use of ice-liquid water potential temperature as a thermodynamic variable in deep atmospheric models. *Mon. Wea. Rev.*, **109**, 1094–1102

Weisman, M. L., and Klemp, J. B. 1982 The dependence of numerically simulated convective storms on vertical wind shear and buoyancy. *Mon. Wea. Rev.*, **110**, 504–520